J Mater Sci (2008) 43:1389–1399
DOI 10.1007/s10853-007-2309-z

A study of S-doped TiO_2 for photoelectrochemical hydrogen generation from water

L. K. Randeniya · A. B. Murphy · I. C. Plumb

Received: 5 April 2007 / Accepted: 12 November 2007 / Published online: 12 December 2007

Abstract Sulfur-doped titanium dioxide (TiO_2) was investigated as a potential catalyst for photoelectrochemical hydrogen generation. Three preparation techniques were used: first ballmilling sulfur powder with Degussa P25 powder (P25), second, ball milling thiourea with P25, and third a sol–gel technique involving titanium (IV) butoxide and thiourea. The resulting powders were heat-treated and thin-film electrodes were prepared. In all three cases, the heat-treated powders contained small amounts of S (1–3%). However, Rietveld analysis on X-ray diffraction (XRD) measurements revealed no significant changes in lattice parameters. For the samples prepared using thiourea, X-ray photoelectron spectroscopy (XPS) measurements indicated the presence of N and C in the heat-treated powders in addition to S. In all cases, visible-ultraviolet spectroscopy performed on bulk powders confirmed the extension of absorption into the visible region. However, the same spectroscopic technique performed on thin-film electrodes ($\sim$0.5 μm) suggests that the absorption coefficients were very small in the visible region ($\leq 10^4$ m^{-1}). The first and third methods yielded powders with substantially smaller photocatalytic activity relative to P25 powder in the UV region. The electrodes prepared from powders obtained using the second method yielded photocurrents comparable to those prepared from P25 powder.

Introduction

For photoelectrochemical hydrogen production, a photoelectrode material is required with an appropriate band gap to harvest as much of the incoming solar radiation as possible. The material needs to have good optical absorption, be stable in strong electrolytes, have efficient electronic charge transfer and suitable energetics (location of conduction and valence band edges), and be inexpensive and readily available. Titanium dioxide (TiO_2) satisfies most of the above requirements. Its main shortcoming is that its relatively large band gap (3.0 eV for the rutile form) means that the fraction of the incoming photons from the sun at the surface of the earth that are able to excite electrons across the band gap is only 2.3%. If the band gap of TiO_2 could be lowered to close to the ideal value for water splitting (approximately 2 eV), without seriously impacting on its favorable energetics, photo-stability, or charge transfer efficiency, it should be possible to approach the US Department of Energy goal of 10% efficiency for photoelectrochemical hydrogen production from sunlight.

There have been many studies investigating the reduction of the band gap of TiO_2 by doping with anions. Asahi et al. [1] calculated densities of states for anatase TiO_2 with substitutional doping of C, N, F, P, or S for O. They found that S-doping produced similar bandgap narrowing to that of N-doping, but suggested that it would be difficult to incorporate S into TiO_2. However, there are several studies in the recent literature which claim that the incorporation of S atoms into the TiO_2 lattice has been achieved [12, 18–21, 32, 35, 36]. It should be noted however that out of all these studies, only one, that of Chandra Babu and Srivastava, [3] investigated the use of S-doped materials for photoelectrochemical hydrogen production.

In the present study, we report the use of three different techniques to obtain S-doped TiO_2 powders and investigate their suitability for efficient water splitting, under both UV and visible illumination. The powders, and electrodes formed from the powders, are characterized by XRD, XPS,

L. K. Randeniya (✉) · A. B. Murphy · I. C. Plumb
CSIRO Materials Science and Engineering, P.O. Box 218, Lindfield, NSW 2070, Australia
e-mail: Lakshman.Randeniya@csiro.au

scanning electron microscopy (SEM), Vis–UV, and Fourier transform infrared (FTIR) spectroscopy, and by electrochemical techniques.

Experimental

Sample preparation

S-doped TiO_2 powders were prepared by three different techniques. The first two techniques involved ballmilling of P25 powder with either sulfur or thiourea. The third method involved a sol–gel preparation technique using titanium (IV) butoxide (tetrabutyl titanate) and thiourea.

Ball-milled materials were prepared in a sealed zirconium oxide canister containing 4−5 zirconium oxide balls and the powder. Ball-milling experiments with S and P25 powder used 0.32 g of S and 4.0 g of P25 (molar ratio of TiO_2 to S of 5:1). Experiments with larger amounts of S in the mixture (up to molar ratio of TiO_2 to S of 1:1) led to powders with similar electrochemical characteristics. For ball milling of thiourea + P25 powder, mixtures with molar ratios of P25: thiourea ranging from 1:4 to 1:0.5 were used.

For the sol–gel method, a mixture of thiourea and TiO_2 was prepared by mixing 34 g (0.1 mol) of tetrabutyl titanate with 7.6 g (0.1 mol) of thiourea in 300 mL ethanol. The solution was stirred magnetically for two hours and allowed to evaporate at room temperature under a fume hood. A white powder was obtained from this procedure. Mixtures with different molar ratios of TiO_2 to thiourea were prepared by changing the amount of thiourea used.

The resulting powders were heat-treated in vacuum in the temperature range of 400 and 600 °C. Ball-milled samples yielded yellow to brown colored powders after heating (typically 30 min to 2 h). Colors tended to fade after longer periods of heating. For sol–gel prepared powders, heating for short periods of time led to black to dark gray powders. Heating for longer periods (>20 h) led to yellow powders.

Coating of powders onto conducting substrates

Electrodes were prepared by coating powders onto FTO (fluorine-doped tin oxide) conducting glass substrates. A dip coating method similar to that of Neumann et al. [17] was used. The suspension consisted of 80 mg powder, 10 mL ethanol, 250 μL acetylacetone, and 150 μL Triton X (polyethylene glycol). Cleaned substrates were dipped and removed at a speed of 1 cm min^{-1}. Following coating, the samples were heat-treated in an air oven at a temperature of 350 °C for 30 min to improve adhesion and remove volatiles. The film thickness was measured using a step-edge profilometer (Sloane Instruments Dektak 3030). Films of thickness ranging from 0.3 to 1 μm were obtained using 8–20 dips.

The dipcoating method was not successful for obtaining electrodes for the powder prepared with the sol–gel method. The resulting films were of uneven thickness and had poor adhesion to the substrate.

Characterization of samples

Preliminary XRD measurements were carried out on heat-treated powders using a Phillips PW 1830 diffractometer with Cu Kα radiation ($\lambda = 0.154056$ nm). For Rietveld analysis, measurements were carried using a Panalytical X'Pert Pro diffractometer with an X'cellerator multichannel detector and a real time multiplier strip. The diffraction patterns were fitted using the software package X'pert HighScore to yield Rietveld data. Transmission electron microscopy (TEM) was conducted using a JEOL 2000FXII instrument operating at 200 keV. The powders were made into small pellets and examined using a JEOL JSM 5400LV scanning electron microscope (SEM) equipped with an energy dispersive X-ray analysis (EDX) system. Vis–UV spectra were obtained using a Varian Cary 5 Spectrophotometer equipped with a diffuse reflectance accessory. Spectra were recorded for both powders and thin films. Both reflectance and transmittance were measured for the thin films on conducting glass substrates; the diffuse reflectance accessory was operated in the total ('S') mode (specular plus diffuse) to allow as much of the transmitted and reflected light as possible to be captured. The absorbance A_λ at wavelength λ was calculated from the reflectance R_λ and transmittance T_λ as $A_\lambda = 1 - R_\lambda - T_\lambda$. XPS measurements were performed on coated samples using a SPECS Sage 150 system, with an Mg Kα source operated at 10 kV and 10 mA emission current. In some cases, the depth profile of elements was obtained by ion milling of samples using a 5 mA argon ion beam for 2 min. Both powders and coated samples were examined by FTIR spectrometry, using a Digilab FTS40 Spectrometer with a glow bar source, a KBr beamsplitter and a liquid nitrogen-cooled MCT detector. The spectrometer was equipped with a Model 091-0608A Universal Sampling Accessory to allow diffuse reflectance measurements in the mid-infrared (400–6000 cm^{-1}, or 1.7–25 μm). Photoelectrochemical measurements were made using a conventional three-electrode arrangement with a Pt wire counter electrode and a saturated calomel electrode (SCE) reference as described elsewhere [14]. The electrolyte (5M KOH solution) was purged with nitrogen prior to and during the measurements. A Voltalab PGZ 3000 potentiostat with a scanning rate of

1 mV s^{-1} was used to measure photocurrents as a function of applied voltage. The light source was a 1000 W ozone-free xenon lamp (Oriel 6271) fitted with an Oriel 61945 water filter. The power density on the electrode was typically 100 mW cm^{-2}. For incident photon to current conversion efficiency (IPCE) measurements, an Oriel Model 7750 monochromator was used.

Nomenclature for samples

The following nomenclature will be used to identify samples. The majority of the results presented in the discussion for ball-milled P25 and S are for samples prepared from 4.0 g of P25 and 0.32 g S ball milled for approximately 12 h. This powder is labeled P25S_1. The majority of the results for ball-milled thiourea and P25 are presented for P25TU_1 (4.0 g P25 and 4.0 g thiourea) and for P25TU_2 (4.0 g P25 and 2.0 g thiourea). The white powders from sol–gel preparation using 34.0 g of tetrabutyl titanate and 7.6 g of thiourea were labeled TBTU_1. Heat-treated powders are identified according to the duration and temperature of heat treatment, for example, P25S_1_500C_2h is a sample of P25S_1 heat-treated at 500 °C in vacuum for two hours.

Results and discussion

Measurements were carried out for powders and for coated samples. The results for powder samples are discussed in Section "Characterization of powders", and those for coated samples in Section "Characterization of coated samples".

Characterization of powders

XRD measurements

XRD measurements on P25 powder, shown in Fig. 1a, confirmed that it consists of approximately 75% anatase and 25% rutile. Figure 1b shows that the anatase component of the P25 powder converts almost completely to rutile during the ball-milling and heat treatment (at 500 °C in air for 2 h) process. The milled samples prior to heat treatment consist of a substantial component of amorphous powder as evidenced by the XRD spectrum (not shown). This occurs whether S is included or not in the ball-milled mixture, in agreement with the findings of Zhang et al. [36]. Rietveld analysis of the powders resulting from heat-treated ball-milled P25 + S gave 85% rutile but showed no apparent shifts in the high angle XRD peaks from the original rutile peaks of the P25 powder to ball-milled powder. This indicates that no significant changes to lattice parameters have occurred. When the TiO_2 to S ratio of the ball-milling mixture was changed from 5:1 to 1:1 the conversion rate of anatase to rutile decreased. The resulting powder after 12 h of milling and after heat treatment was found to contain 55% rutile rather than 85%.

Figure 1c shows the XRD spectra for ball-milled P25 + thiourea powder (TiO_2 to thiourea ratio of ~1:1 in the original mixture) following heat treatment in vacuum at 500 °C for 2 h. These measurements indicate that the conversion of the anatase component to rutile during the milling process is much slower in this case. This result was found to be true for powders with molar ratios of TiO_2: thiourea ranging from 1:4 to 1:0.5. For the mixture with the lowest amount of thiourea (TiO_2 to thiourea ratio of 1:0.5 in the original mixture), the rutile composition increased to only ~ 30% after 12 h of milling. Rietveld analysis of the spectra revealed that there were no significant changes to the lattice parameters in the ball-milled powder.

XRD data for the sol–gel prepared powder heat-treated under vacuum for 24 h at 500 °C is shown in Fig. 1d. The sol–gel powder consists of anatase, with no significant rutile component. The spectra show no evidence of change in lattice parameters of the sol–gel powder with respect to pure anatase.

Vis–UV spectroscopy

Figure 2 shows diffuse reflectance spectra for selected samples obtained from the three preparation methods. All samples show substantial absorption at wavelengths beyond 420 nm. The absorption in the visible region generally increases with heat treatment temperature and is highest for samples heat-treated in the 500 °C–600 °C range. Heating ball-milled samples for longer periods (more than 4 h) leads to a gradual decrease in the visible absorption. For sol–gel powders, heating for 22 h yielded powders with the absorption characteristics shown in Fig. 2. Powders prepared from different molar ratios of precursor compounds specified in the experimental section but subjected to the same heat treatment conditions showed similar absorption spectra. This indicates that the reactant containing sulfur is in excess in the mixtures used.

FTIR spectroscopy

The IR diffuse reflectance spectra (Fig. 3) for powder samples of P25 and P25S_1_500_2h were found to be essentially the same except for some minor differences in wave numbers below 1300 cm^{-1}. Differences at long wavelengths may be due to conversion of anatase to rutile

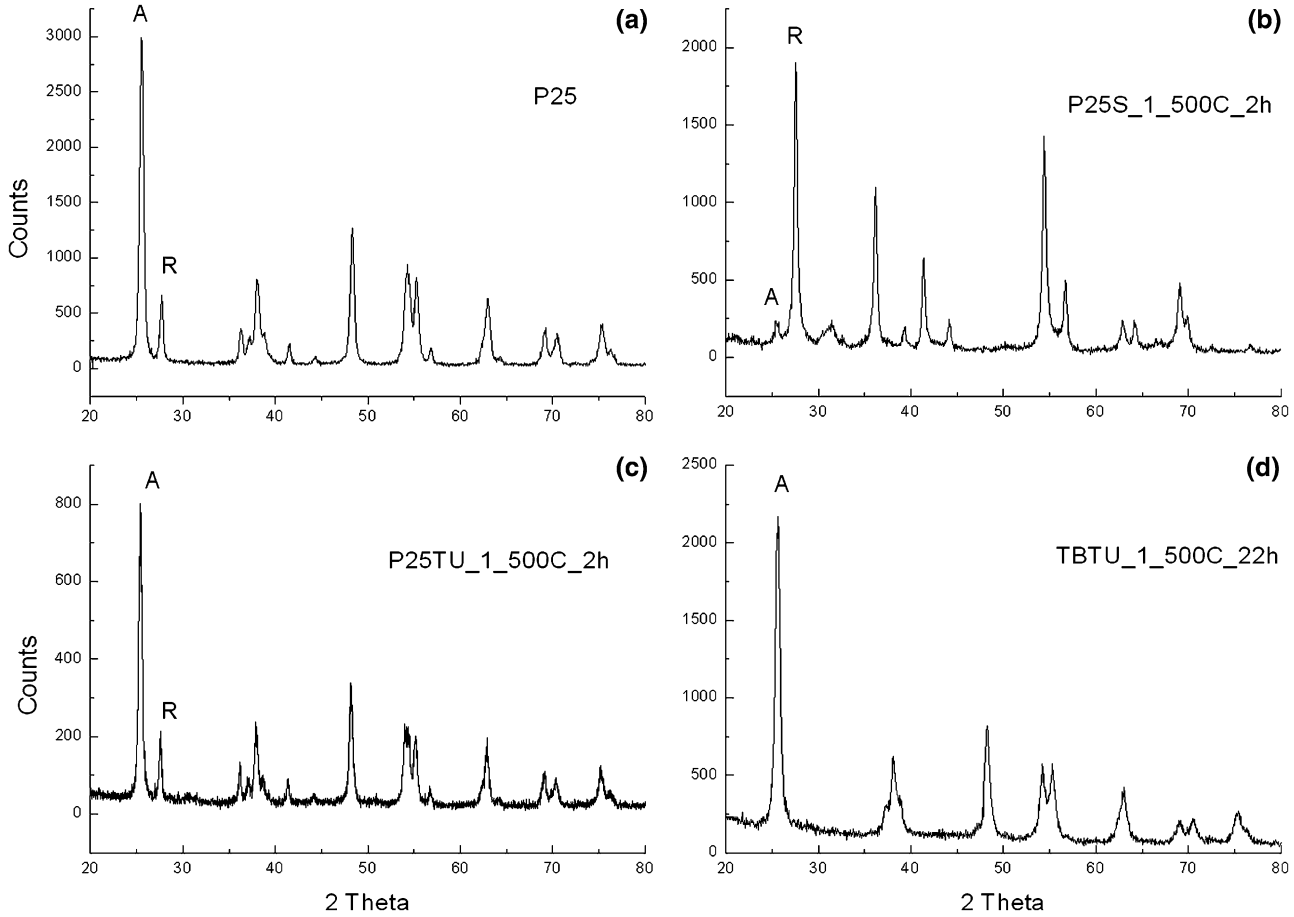

Fig. 1 XRD spectra for (**a**) P25 powder; (**b**) ball-milled P25 + S (molar ratio of TiO_2 to S of 5:1) powder heat-treated in vacuum at 500 °C for 2 h (P25S_1_500C_2h); (**c**) ball-milled P25 + thiourea powder heat-treated at 500 °C for 2 h (P25TU_1_500C_2h) and (**d**) sol–gel powder heat-treated at 500 °C for 22 h (TBTU_1_500C_22h). Anatase (101) and rutile (110) peaks are labeled and can be used for a quick assessment of relative amounts of the two phases present in the powders

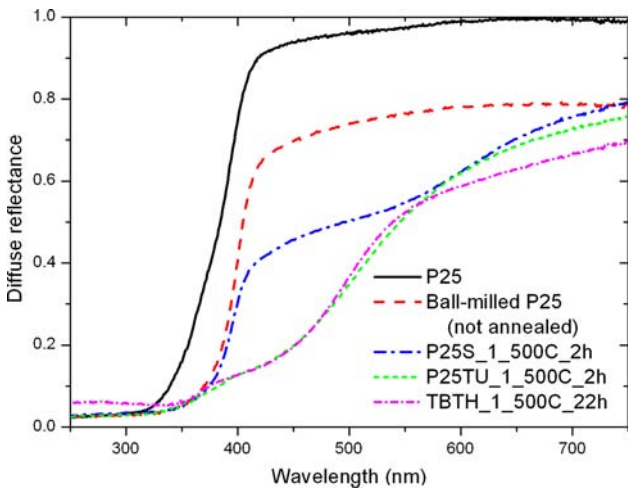

Fig. 2 Vis–UV diffuse reflectance spectra for powders

in the ball-milling process. Rutile absorbs strongly at wave numbers less than about 900 cm^{-1}. There is also an asymmetric stretch of SO_2 at around 1390 cm^{-1} [29], but the features at these wavelengths are not sufficiently strong to assign them unambiguously.

The spectra of heat-treated ball-milled samples of TiO_2 and thiourea show a peak at 2045 cm^{-1} (Fig. 3). The peak is present in samples heat-treated for 2 h and in samples heat-treated for 22 h. Grey et al. [9] reported peaks in the range 2050–2200 cm^{-1} for nanophase TiO_2 prepared by hydrolysis of thiourea and tetrabutyl titanate, which they assigned to –NCS, –NCO, or –CN bands. Mitchell and Williams [13] examined the infrared spectra of a number of inorganic thiocyanates between 2000 and 2200 cm^{-1}, noting that the position of the absorption band depends on the nature of bonding of the ligand to the central cation. The CN stretching frequency is at lower frequencies, (2060−2150 cm^{-1}) in the isothiocyanates R−NCS, than in the thiocyanate R−SCN, (∼2140 cm^{-1}). On the basis of these earlier studies, and the lack of other possible assignments at the frequency of the observed absorption feature, it seems likely that the 2045 cm^{-1} feature is due to the presence of organic species in the powder samples, and

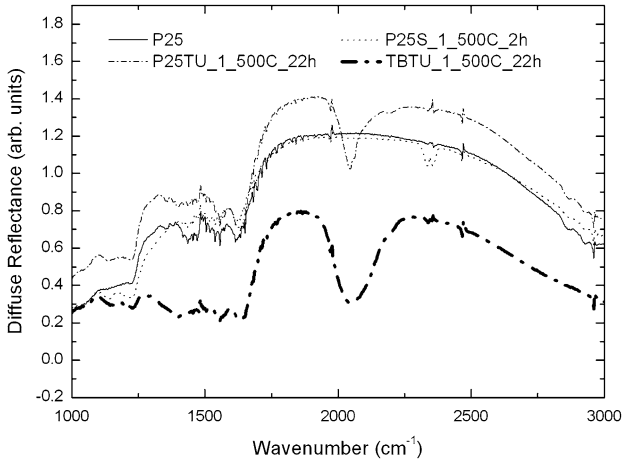

Fig. 3 Diffuse reflectance FTIR spectra for powders

that the bonding is more likely to be isothiocyanate than thiocyanate. This particular peak is even stronger (Fig. 3) for the heat-treated sol–gel powder, TBTU_1_500C_22h, and the peak absorption occurs at slightly greater wave number of 2050 cm^{-1}. This difference may not be significant, given the possible effect of the slope of the underlying broad absorption on peak positions. It is concluded that more organic material is present in the sol–gel material than in the ball-milled material, resulting in stronger absorption.

TEM and EDX measurements

TEM images obtained for heat-treated powders prepared using the ball-milling technique show that the nano-size particles are well separated in both samples. Similar results were obtained for the sol–gel prepared samples.

Quantitative measurements using EDX also confirmed that some Zr was incorporated into the mixture during the milling process. As expected, the atomic ratio of Zr to Ti in the mixture increased with milling time. Typical values for atomic ratios determined for various heat-treated samples are shown in Table 1. The SEM electron beam activates a volume of the sample to a depth of approximately 1 μm in the pressed powders.

Table 1 Results of quantitative measurements of elemental composition (atomic%) of pressed powders using SEM

	Ti	Zr	S
Ball-milled P25	0.90–0.98	0.09–0.01	0.0
P25S_1_500C_2h	0.92–0.98	0.05–0.005	0.01–0.03
P25TU_1_500C_2h	0.98	<0.001	0.01
TBTU_1_500C_2h	0.98–0.99	0.0	0.01–0.002

The impact of Zr contamination is not known. However, comparison of Vis–UV results for ball-milled P25 powder and ball-milled P25 + S powder indicate that the change in the absorption characteristics of the P25 powder is caused by S (in the case of ball-milled P25 + S) and/or other dopants such as N and C in the other two preparations, rather than Zr.

Characterization of coated samples

Photoelectrochemical measurements (Section "Photoelectrochemical studies") showed clearly that the photocurrents vary with the thickness of the film. The largest photocurrents were obtained for film thickness in the range of 500–800 nm. The optimum coating thickness is determined by a balance between the requirement to maximize the absorption of incident photons, and the requirement that those charge carriers that are produced reach the electrolyte [14]. The results presented in the following sections were obtained using electrodes with films approximately 600 nm thick coated onto conducting glass.

XPS spectroscopy

There are some inconsistent assignments of XPS peaks for S and N in the literature for doped TiO_2 powders. A brief literature review of current understanding for the assignment of S and N peaks for such compounds is presented in the Appendix. Figure 4a shows the XPS spectrum in the S 2*p* region for a dip-coated electrode of heat-treated ball-

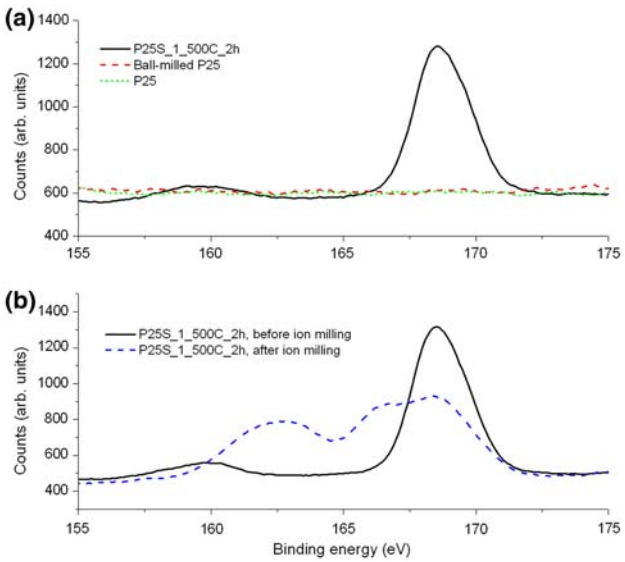

Fig. 4 (**a**) S 2*p* region of the XPS spectrum for P25, ball-milled P25, and P25S_1_500C_2h electrodes; (**b**) XPS spectrum for P25S_1_500C_2h before and after ionmilling for 2 min

milled S and TiO_2, P25S_1_500C_2h. Also shown are the spectra for electrodes coated with P25 powder (unheated) and ball-milled P25 (unheated). The peak at 168.4 eV for P25S_1_500C_2h is most likely due to SO_4^{2-} (S^{6+}) ions in the TiO_2 lattice. This peak and the visible absorption disappear when the powder is heated at 800 °C. On this basis, we hypothesize that the extension of absorption into the visible region is caused by the presence of SO_4^{2-} ions in the titanium dioxide lattice. A quantitative analysis of the XPS peaks yields 4.2 atom% for S. This is slightly higher than 1–3 atom% values determined for S from the EDX measurements (Table 1). This may be due to the fact that XPS measures the properties of the top 3–5 nm of the film, whereas EDX measures to a depth of about 1 μm.

Figure 4b shows the effect of ion milling with an argon ion beam for two minutes on the S 2*p* feature of a ball-milled P25 and sulfur-coated electrode. Ion milling leads to a reduction in size of the SO_4^{2-} peak at 168.5 eV, and the formation of additional peaks at 163 and 166.5 eV. Using Table A1 in the Appendix, it can be seen that the 163 eV peak is associated with Ti–S bonds, and the other peak possibly with SO_3^{2-} bonds. Spectra obtained with ion-milled samples have to be treated with caution, since the energy of the ion beam can cause chemical changes in the sample. It is very likely that these bonds are formed by the ion-milling process, and do not represent species that exist below the surface of the electrode coatings.

The sulfur content is approximately equal in the ion-milled and unmilled coatings, suggesting that the sulfur is present throughout the coating. However, since the coatings are made of nanoparticles, there are surfaces available for chemisorption throughout the film, and it is possible that the sulfur is present only on the surface of these particles. The ion-milling depth in these experiments is not known, but the milling rate is likely to be of the order of a few nm per minute.

Figure 5a and b show the S 2*p* and N 1*s* regions, respectively, for two of the electrodes coated with ball-milled P25 and thiourea powder P25TU_1 heat-treated for different lengths of time (P25TU_1_500C_2h and P25TU_1_500C_22h). Spectra for P25 and ball-milled P25 are shown for comparison. The electrode coated with the powder heat-treated for 2 h has a strong S 2*p* peak at 168–169 eV, which can be assigned to SO_4^{2-} ions. The same peak was seen in the ball-milled P25 + S samples. The amount of S in the first few nm of the film is measured to be 1 atom%. A similar percentage value for the sulfur content of the powder was estimated from the EDX measurements. The electrode coated with the powder heat-treated for 22 h does not show this peak; this is correlated with a decrease in visible absorption of the powder.

The N 1*s* region shows similar peaks for all electrodes: a large peak at 400 eV, a smaller peak at 409 eV to 410 eV,

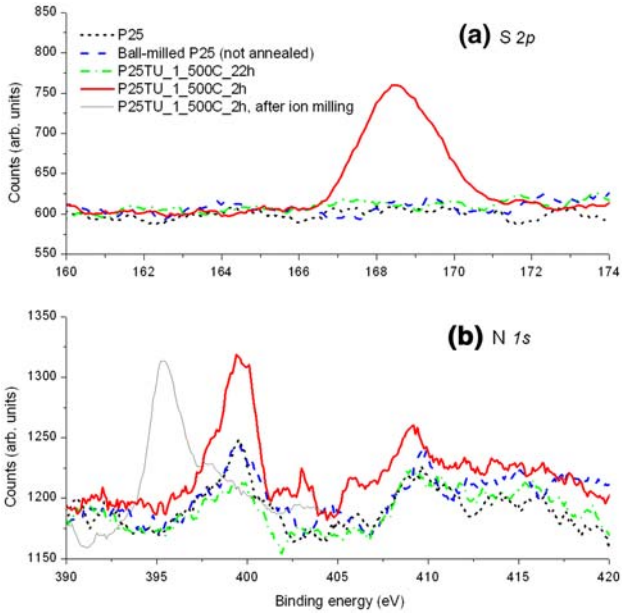

Fig. 5 Regions of the XPS spectra for ball-milled P25 + thiourea samples, (**a**) S 2p and (**b**) N 1s. Corresponding spectra for P25 and ball-milled P25 are shown for comparison

and broad peak centerd at 414 eV to 415 eV. The first peak could be assigned to either chemisorbed N_2, or hyponitrite ($N_2O_2^{2-}$) ions (see Appendix). The presence of an O 1*s* peak at 531–532 eV (not shown) indicates that this is likely to be a hyponitrate peak (see Appendix). The other two N 1*s* peaks can be assigned to nitrite (NO_2^-) ions. The peaks, particularly the peak at 400 eV, are significantly larger for the electrode coated with powder ball-milled for 2 h. The nitrogen content of this film is 2.5 atom%, compared to between 1.2% and 2.2% for the other three films shown in Fig. 5a.

It is interesting that all samples show nitrogen contents of at least 1 atom%, and peaks corresponding to hyponitrite and nitrite species. As noted in the Appendix, several studies have demonstrated the occurrence of photo-oxidative nitrogen fixation on UV-illuminated TiO_2 surfaces [2]. These studies show that UV radiation can cause absorbed nitrogen to be oxidized to hyponitrite anions, which can be further oxidized to nitrite anions and nitrate anions. While some of the samples have been exposed to xenon arc lamp radiation during measurements within the photocatalytic cell, the ball-milled P25 sample was not thus exposed to UV radiation. Hence, the presence of the hyponitrite and nitrite peaks appears to be an intrinsic property of the samples.

The FTIR measurements presented in Section "FTIR spectroscopy" indicate the possible presence of isothiocyanate (CNS) in heat-treated P25TU powders. The NIST database [33] indicates that the N 1*s* XPS feature for KCNS and NaCNS is expected at around 398 to 399 eV, and the S 2*p* feature for NH_4CNS at around 161 eV. Ciszek et al. [6]

find the S 2*p* feature for thiocyanate (SCN) at 165 eV. It is possible that an isothiocyanate feature is present in the N 1*s* spectrum, but there is no evidence of the corresponding feature in the S 2*p* spectrum; indeed there were no observable sulfur peaks for the electrode made with the ball-milled P25 and thiourea sample heated for 22 h. Hence the XPS measurements do not give any evidence of the presence of isothiocyanate in electrodes prepared using P25TU powders.

Figure 5b shows the effect of ion milling, by sputtering with an argon ion beam, on the N 1*s* region, of a ball-milled P25 + thiourea electrode. The N 1*s* peak at 400 eV, corresponding to hyponitrite or molecular nitrogen, is greatly reduced, and a peak at around 396 eV, corresponding to Ti–N bonds (see Appendix) appears. Some authors [30] have interpreted the presence of this latter peak in ion-milled samples of N-doped TiO_2 as evidence of the presence of Ti–N bonds in the samples. However, it is most likely that the Ti–N bonds are in fact formed by the ion-milling process.

The nitrogen content is approximately equal in the ion-milled and unmilled coatings, as was observed for the sulfur content in the ball-milled P25 and sulfur coatings. This indicates that the nitrogen is present throughout the coating. It is possible, however, that the nitrogen is present only on the surface of the particles forming the coating.

As discussed earlier, it was difficult to coat the heat-treated sol–gel powder TBTU_1_500C_22h onto a substrate, and only a patchy coating was obtained. XPS measurements of the coating indicated that the sulfur content was about 1%, in agreement with EDX measurements (1–2 atom%) and the nitrogen content was about 4%. A peak for S 2*p* at 168 eV was observed, consistent with SO_4^{2-} ions. A strong N 1*s* peak at 399.5 eV, corresponding to hyponitrite or molecular nitrogen, was also observed; the presence of an O 1*s* peak between 531 eV and 532 eV suggests the peak is due to hyponitrite ions.

In summary, all electrodes made from doped powders, except that from ball-milled P25 and thiourea powder heat-treated for 22 h, show an S 2*p* peak corresponding to SO_4^{2-} ions. Further, all electrodes show N 1*s* peaks corresponding to $N_2O_2^{2-}$ and NO_2^- ions; these peaks are strongest for samples made from ball-milled P25 and thiourea powder heat-treated for 2 h.

FTIR spectroscopy

Examination of the IR spectrum of coated samples (not shown) did not reveal the 2045 cm^{-1} absorption feature found for the powdered samples prepared using thiourea. This could be due to the fact that the sensitivity of the FTIR instrument is not sufficient to detect the organic component in the small volumes of material present in the thin films, or that the organic material might have been removed either in the coating process (by dissolving in ethanol) or in the subsequent heat treatment in air. To test these possibilities, a powder sample of ball-milled P25 + thiourea was rinsed in ethanol, followed by overnight drying in an air oven at 125 °C to remove the ethanol. This procedure should have removed any ethanol-soluble component. A second powder sample was subjected to heat treatment in air at 400 °C. Finally, a dip-coated sample which had not been subjected to the 400 °C heat treatment was examined. The ethanol treatment produced no significant change in the absorption of the powder at 2045 cm^{-1}. Heat treatment of the powder produced a slight decrease in the absorption at 2045 cm^{-1} (up to a factor of 2), but the feature was still readily detectable. No absorption could be detected for the coated sample not subject to the air heat treatment step. On the basis of these observations, it seems most likely that the reason that the isothiocyanate peak cannot be detected in the coated samples is that the FTIR instrument does not have sufficient sensitivity. The organic component is still expected to be present in the coated samples, even after heating for 22 h under vacuum.

Photoelectrochemical studies

Figure 6 shows the photocurrents obtained from electrodes dip-coated with powders produced by the three different preparation techniques as a function of potential between the working and the reference electrodes. Also shown are the photocurrents obtained from electrodes coated with P25 powder and ball-milled P25 powder. The photocurrents

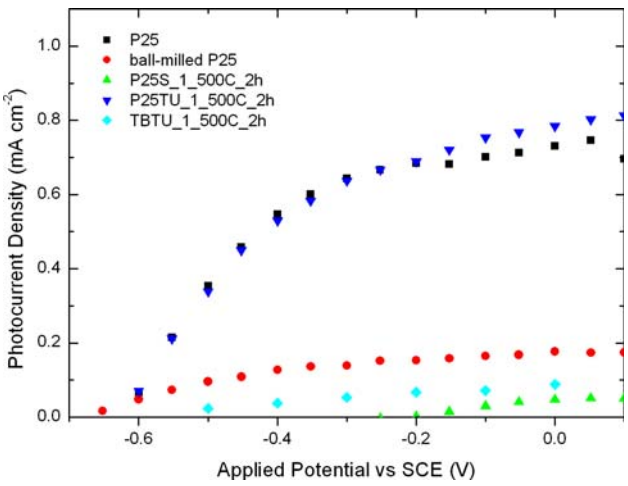

Fig. 6 Measured photocurrent density as a function of applied potential for electrodes prepared from various powders. Lamp intensity at electrode = 100 mW cm^{-2}

obtained from ball-milled P25 + thiourea powder (P25TU_1_500C_2h) were very similar to those of P25 and together they were the best performing electrodes in terms of photocurrent generation. It is clear that the photocurrents obtained from electrodes coated with ball-milled P25, ball-milled S + P25 (P25S_1_500C_2h), and sol–gel (TBTU_1_500C_22h) were all substantially lower. Anodic current onset potentials were similar for electrodes prepared from P25 and ball-milled P25 powders (~ -0.6 V with respect to SCE), and for those prepared from ball-milled P25 + thiourea. For the electrode prepared from ball-milled P25 + S, anodic current onset occurred at a more positive voltage (~ -0.2 V with respect to SCE).

It is clear that ball milling the P25 powder reduces the photocurrents substantially. This could be due to a number of factors including the change in the composition of the powder (to mainly rutile) and the change in surface and size characteristics of the particles during the milling process. Heat treatment of the ball-milled P25 powder (500 °C for 2 h) led to a small improvement ($\sim 10\%$) in the photocurrents.

The ball-milled P25 + S samples have photocurrents even lower than those obtained for the ball-milled P25-coated electrodes. The maximum photocurrent densities of 60–80 μA cm^{-2} measured for P25 + S samples are in broad agreement with the values obtained by Neumann et al. [17] for doped powders ($\sim$ 30 μA cm^{-2} at a power density of 36 mW cm^{-2}). They argued that such marginal photocurrents could be due to trap-filling processes and the photo-generated holes relaxing rapidly into defect states without initiation of oxygen evolution. The ball-milling process invariably leads to surface imperfections, which can lead to the formation of defect states and diminish the photocatalytic activity of the material.

The ball milling of P25 and thiourea resulted in powders with similar photocurrents to those for P25. Electrodes prepared with powders heat-treated for up to 22 h gave similar results. As revealed by the XRD results presented earlier, the conversion of anatase to rutile is much slower during the ball milling of thiourea with P25. It could be that the local temperature increases upon impact within the milling medium are much smaller in this case. Therefore, it is possible that there has been little change in the composition and morphology of P25 during the milling process. Thiourea thermally dissociates at a temperature of 200–230 °C with an activation energy of 89.8 kJ mol^{-1} and a Gibbs free energy change of 140 kJ mol^{-1} [34]. Adsorption of either the thiourea or one or more of the decomposition products (CS_2, HNCS, and NH_3) onto the surface of the P25 may act as a lubricant, limiting the temperature rise of the P25 particles during ball milling. Particularly for the powders heat treated for 2 h, the XPS measurements indicate the presence of C, S, and N in the films and the Vis–UV spectrum indicates the presence of visible absorption, possibly due to states within the band gap. If the trap states are present due to incorporation of S and N, they are not detrimental to photocurrent in the UV region, unlike the case of P25 + S powders.

The lower currents obtained from the sol–gel-prepared electrodes may be due to the poor quality of the electrode. The coating flaked off easily during measurements. Therefore the photocurrents measured may not be a true reflection of the quality of the sol–gel-prepared powder as a photocatalyst.

Measurement of IPCE as a function of wavelength allows determination of the extent of photocatalytic activity in the visible region. Figure 7 shows IPCE measurements for electrodes prepared from P25 and ball-milled P25 + thiourea powders. It can be seen that there is no evidence of visible light conversion for the electrode prepared from ball-milled P25 + thiourea powder as the IPCE is essentially zero beyond the band gap of rutile TiO_2 (413 nm).

The photocurrents were too small for the measurement of IPCE curves for the electrodes prepared from ball-milled P25 + S and sol–gel powders. Therefore a long-pass filter with a cut-off of 435 nm between the lamp and the ball-milled P25 + S sample was employed to determine the photoactivity in the visible region. For the electrodes prepared from P25 + S powders, the resulting photocurrents with the filter present were found to be 2–5% of the photocurrents without the filter present. Hence, there is some visible activity of this material, although the visible light efficiency is very small.

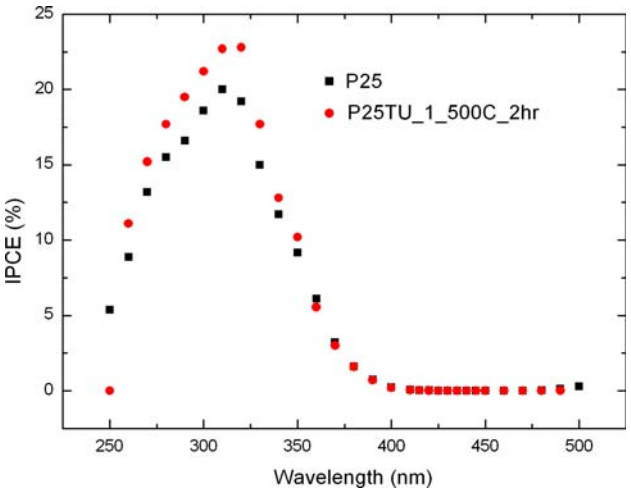

Fig. 7 IPCE measurements for electrodes prepared from P25 and P25TU_1_500C_2h powders. Measurements were made at an applied potential of −.4 V with respect to reference electrode (SCE)

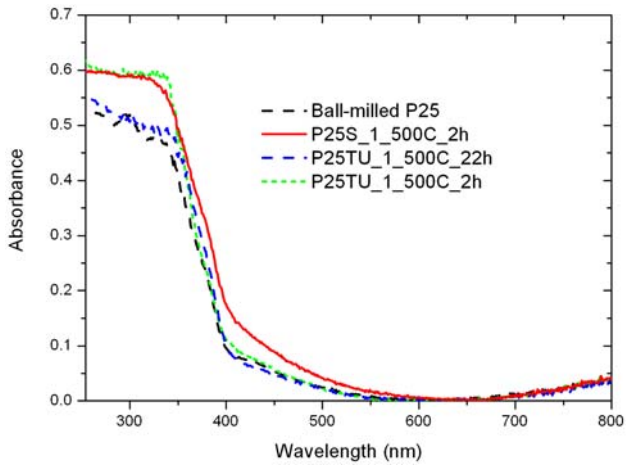

Fig. 8 Vis–UV absorbance for electrodes with optimum thicknesses for photocurrent generation (approximately 0.6 μm)

Vis–UV measurements

The strong absorption in the visible region shown in Section "Vis–UV spectroscopy" was obtained for the powders compacted into 1 mm thick samples. In the case of electrodes, however, the coating is much thinner.

In Fig. 8, the absorption as a function of wavelength is shown for electrodes prepared from ball-milled P25 + S and ball-milled P25 + thiourea powders. It can be seen that there is little increase in the visible absorption between the P25 and the ball-milled samples. Thicker coatings show more appreciable absorption (not shown in Fig. 8) beyond the band gap of anatase. These results indicate that the UV absorption of the ball-milled powders is sufficiently strong for a submicron film to absorb most of the incident light, indicating an absorption coefficient of greater than 10^6 m^{-1} at UV wavelengths. However, at 450 nm, only a small fraction (<3%) of the visible light is absorbed in a submicron film, and about 10% in a 10 μm film. This suggests that the absorption coefficient is of order 10^4 m^{-1} at this wavelength for ball-milled P25 + S and ball-milled P25 + thiourea samples

Conclusions

In the present study, three different techniques have been used to dope TiO_2 with sulfur. In all cases, the powders showed absorption in the visible portion of the spectrum, extending, in some cases, to beyond 700 nm. However, when the powders were coated onto conducting glass, it was found that a coating thickness of several micrometers was required before a significant fraction of the visible radiation was absorbed by the film. Films of thickness around 0.5–0.8 μm, which were found to give the largest photocurrents, showed very weak absorption of visible light, which would not be expected to contribute significantly to the photocurrent. All coatings showed the presence of nitrogen in the form of hyponitrite and nitrate ions and sulfur in the form of sulfate ions, except after very long heat treatment.

Our results do not provide evidence that S-doped TiO_2 photocatalysts generate hydrogen more efficiently than undoped TiO_2, under either UV radiation or under the full spectrum from a xenon lamp. This contrasts with reports of increased performance in the oxidation of some organic chemicals. There are two reasons for this: first, anion doping creates trap states, which adversely affect water splitting but not oxidation reactions with lower energy requirements. Further, water splitting requires the photocatalytic powder be coated onto an electrode, to ensure that the production of hydrogen and oxygen are spatially separated. Powder suspensions may be optically thick enough to absorb a significant amount of visible radiation, but the thin-film electrodes which give the highest photocurrents for photoelectrochemical hydrogen production do not absorb sufficient visible photons to generate appreciable photocurrents from visible radiation.

Acknowledgements We are grateful to Dr John Dunlop for assistance with ball milling, and in the interpretation of XRD and SEM measurements, Drs Phil Martin and Avi Bendavid for assistance with XPS measurements, Dr Bin Yang and Dr Victor Luca (Australian Nuclear Science and Technology Organization) for performing the Rietveld analyses and TEM measurements, respectively, and Ms Julie Glasscock for assistance in coating samples and for thickness profiling of coated electrodes.

Appendix

Assignment of XPS peaks

Sulfur peaks

The identification in the literature of S 2*p* peaks from XPS data has not always been consistent. While a peak at around 163 eV has been consistently identified as S^{2-} species, such as occur with Ti–S bonds [10]; different authors have identified a peak at around 168 eV as S^{6+}/S^{4+} species, or alternatively as adsorbed SO_2.

Umebayashi et al. [31] referred to two articles by Onishi et al. and Sayago et al. [22, 28] to support their identification of the peak as absorbed SO_2. The former article in fact identifies this peak as SO_3^{2-} (i.e., S^{4+}). The latter article, discussed below, provides a survey of different literature values. Zhang et al. [36] who also identified a peak at 169 eV as adsorbed SO_2, referred to one of the above articles [22] and to a paper [10] that is concerned

Table 2 Range of S $2p_{3/2}$ binding energies reported for sulfur species on oxide surfaces

Compound type	Binding energy range (eV)
Sulfides (S^{2-})	162.1–163.6
S_n	162.4–164.8
SO_2 (chemisorbed)	163.5–165.7
SO_3^{2-} (S^{4+})	164.9–167.6
SO_4^{2-} (S^{6+})	166.1–169.0
SO_2 (physisorbed or multilayers)	166.6–171.0

After Sayago et al. [28]

only with a peak at around 163 eV, which is identified as an S^{2-} peak.

Sayago et al. [28] collected literature values of S 2*p* peaks for S-based species absorbed on different surfaces, mainly oxides. Their results are shown in Table 2. They noted that there is a large variation of reported values, because the bonding of the SO_2 molecule is strongly substrate-dependent for oxide surfaces.

Sayago et al. [28] referred to by articles Rodriguez et al. [25] and Polcik et al. [23] as a basis for identification of the physisorbed/multilayer SO_2 peak. Rodriguez et al. [24] observed a peak corresponding to physisorbed SO_2 between 168 and 171 eV in experiments in which a single-crystal ZnO surface was exposed to SO_2 at 110 K. However, these molecules desorbed upon heating to 150 K, and an SO_3^{2-} peak was formed. Moreover, no peaks corresponding to physisorbed SO_2 were observed when polycrystalline ZnO films or powders were exposed to SO_2. Polcik et al. [23] observed similar behavior when platinum was exposed to SO_2 at 90 K. An XPS peak corresponding to multilayer SO_2 was observed at 166.4 eV; however, the peak disappeared and was replaced by an SO_4^{2-} peak when the substrate was heated to room temperature.

The temperatures reached in ball-milling experiments are much greater than those at which physisorbed SO_2 becomes desorbed from single-crystal and metallic surfaces. Moreover, TiO_2 that is ball-milled with the sulfur compounds is in powder form. Hence, the possibility that the peak at around 168 eV observed in such experiments is associated with physisorbed SO_2 can be rejected. The peak should be identified as either SO_3^{2-} (S^{4+}) or SO_4^{2-} (S^{6+}); such peaks have been observed on oxides in single-crystal, polycrystalline, and powder form, and are present at temperatures up to at least 600 K. For example, Rodriguez et al. [24] identified SO_3^{2-} and SO_4^{2-} peaks resulting from exposure of polycrystalline ZnO to SO_2 at temperatures up to 500 K. They found that SO_3^{2-} and SO_4^{2-} resulted from the reaction of SO_2 with oxygen sites. Rodriguez et al. [24] observed an SO_x peak originating from exposure of single-crystal TiO_2 to sulfur. A peak associated with S atoms bonded to Ti rows on the surface was also observed; this disappeared upon heating to 550 K.

Table 3 N 1*s* binding energies reported for oxidized nitrogen species on TiO_2 surfaces after Navio et al. [15]

Compound type	Binding energy (eV)
Hyponitrite ($N_2O_2^{2-}$)	399.8
Nitrite (NO_2^-)	409.6 and 415.6
Nitrate (NO_3^-)	407.3

Nitrogen peaks

Two main N 1*s* peaks have been observed in XPS measurements of nitrogen-doped TiO_2. A peak between 396 and 397 eV has been consistently identified as being due to Ti–N bonds (e.g., [1, 7, 11, 30]). The identification of this peak is based on an XPS study of TiN oxidation chemistry [26].

The second peak, around 400 eV, is generally assigned to molecularly chemisorbed N_2, (e.g., [1, 5, 11]), again based on Saha and Tompkins's study [26]. However, the peak at 400 eV has also been assigned to hyponitrite ($N_2O_2^{2-}$) species, [27] to the presence of NH_x species, [7] and to organic compounds. [8] The hyponitrite peak has been identified in studies of photo-oxidative nitrogen fixation on UV-illuminated TiO_2 surfaces [2, 15, 16]. These studies show that adsorbed nitrogen is oxidized to hyponitrite anions ($N_2O_2^{2-}$), which can be further oxidized to nitrite anions (NO_2^-) and nitrate anions (NO_3^-). The binding energies of these peaks are given in Table 3.

Oxygen peaks

The O 1*s* peak corresponding to Ti–O bonds occurs at 530 eV [26]. Navio et al. [16] have identified a further peak at 531.7 ± 0.1 eV corresponding to adsorbed hyponitrite species. Studies of SO_2 absorption on metal and oxide surfaces [4, 25] have identified a peak at around 531.5 eV that has been assigned to SO_3^{2-} species.

References

1. Asahi R, Morikawa T, Ohwaki T et al (2001) Science 293:269
2. Bickley RI, Jayanty RKM, Navio JA et al (1991) Surface Sci 251–252:1052
3. Chandra Babu KS, Srivastava ON (1988) Cryst Res Technol 23:555
4. Chaturvedi S, Rodriguez JA, Jirsak T et al (1998) J Phys Chem B 102:7033
5. Chen SZ, Zhang PY, Zhuang DM et al (2004) Catal Commun 5:677

6. Ciszek JW, Keane ZK, Cheng L et al (2006) J Am Chem Soc 128:3179
7. Diwald O, Thompson TL, Zubkov T et al (2004) J Phys Chem B 108:6004
8. Gopinath CS (2006) J Phys Chem B 110:7079
9. Grey I, Madsen I, Bordet P, Wilson N, Li C (2005) In: White T et al. (ed) Advances in Ecomaterials, vol 1, Electrochemistry and Catalysis. Stallion Press, Singapore, p 35
10. Hebenstreit ELD, Hebenstreit W, Diebold U (2001) Surf Sci 470:347
11. Li D, Haneda H, Hishita S et al (2005) Mater Sci Eng: B 117:67
12. Liu H, Gao L (2004) J Am Ceram Soc 87:1582
13. Mitchell PCH, Williams RJP (1960) J Chem Soc 1912
14. Murphy AB, Barnes PRF, Randeniya LK et al (2006) Int J Hydrogen Energy 31:1999
15. Navio JA, Cerrillos CC, Real C (1996) Surf Interface Anal 24:355
16. Navio JA, Real C, Bickley RI (1994) Surface Interface Anal 22:417
17. Neumann B, Bogdanoff P, Tributsch H et al (2005) J Phys Chem B 109:16579
18. Ohno T, Akiyoshi M, Umebayashi T et al (2004) Appl Catal A: Gen 265:115
19. Ohno T, Mitsui T, Matsumura M (2003) Chem Lett 32:364
20. Ohno T, Tsubota T, Nishijima K et al (2004) Chem Lett 33:750
21. Ohno T, Tsubota T, Toyofuku M et al (2004) Catal Lett 98:255
22. Onishi H, Aruga T, Egawa C et al (1988) Surf Sci 193:33
23. Polcik M, Haase J, Wilde L et al (1997) Surf Sci 381:L568–L572
24. Rodriguez JA, Hrbek J, Chang Z et al (2002) Phys Rev B 65:Article No. 235414
25. Rodriguez JA, Jirsak T, Chaturvedi S et al (1999) Surf Sci 442:400
26. Saha NC, Tompkins HG (1992) J Appl Phys 72:3072
27. Sakthivel S, Janczarek M, Kisch H (2004) J Phys Chem B 108:19384
28. Sayago DI, Serrano P, Bohme O et al (2001) Surf Sci 482:9
29. Shimanouchi T (1977) J Phys Chem Ref Data 6:993
30. Suda Y, Kawasaki H, Ueda T et al (2004) Thin Solid Films 453–54:162
31. Umebayashi T, Yamaki T, Itoh H et al (2002) Appl Phys Lett 81:454
32. Umebayashi T, Yamaki T, Yamamoto S et al (2003) J Appl Phys 93:5156
33. Wagner CD, Naumkin AV, Kraut-Vass A, Allison JW, Powell CJ, Rumble JR Jr (2003) NIST X-ray photoelectron spectroscopy database, NIST standard reference database 20, Version 3.4 (Web Version) [Web Page]. Available at http://srdata.nist.gov/xps/index.htm
34. Wang S, Gao Q, Wang J (2005) J Phys Chem B 109:17281
35. Yu JC, Ho W, Yu J et al (2005) Environ Sci Technol 39:1175
36. Zhang Q, Wang J, Yin S et al (2004) J Am Ceram Soc 87:1161